11th International Symposium on Turbulence and Shear Flow Phenomena (TSFP11)
Southampton, UK, July 30 to August 2, 2019

SECONDARY FLOW STRUCTURE ASSOCIATED WITH INTERACTING 3D BEDFORMS

Nathaniel Bristow
Department of Aerospace and Mechanical Engineering
University of Notre Dame
Notre Dame, Indiana, USA
nbristow@nd.edu

Gianluca Blois
Department of Aerospace and Mechanical Engineering
University of Notre Dame
Notre Dame, Indiana, USA
gblois@nd.edu

James Best
Departments of Geology, Geography and GIS, Mechanical Science and Engineering
and Ven Te Chow Hydrosystems Laboratory
University of Illinois
Champaign, Illinois, USA
jimbest@illinois.edu

Kenneth Christensen
Departments of Aerospace & Mechanical Engineering and Civil & Environmental
Engineering & Earth Sciences
University of Notre Dame
Notre Dame, Indiana, USA
christensen.33@nd.edu

ABSTRACT

Barchan dunes are three-dimensional, crescent shaped bedforms found in both aeolian and subaqueous environments, including deserts, river beds, continental shelves, and even the craters of Mars. The evolution of and dynamics associated with these mobile bedforms involve a strong degree of coupling between sediment transport, morphological change, and flow, the last of which represents the weakest link in our current understanding of barchan morphodynamics. Their three-dimensional geometry presents experimental challenges for measuring the full flow field, particularly around the horns and in the leeside of the dunes. In this study we present measurements of the turbulent flow surrounding fixed barchan dune models in various configurations using particle-image velocimetry in a refractive-index-matching flume environment. The refractive-index-matching approach enables near-surface measurements, as well as access to the the whole flow field by rendering the solid models invisible. While experiments using solid models are unable to directly measure sediment transport, they allow us to focus solely on the flow physics and full resolution of the turbulent flow field in ways that are otherwise not possible in mobile bed experiments. The results presented here involve spectral analysis of flow in the wake of an isolated barchan, as well as in the interdune region of interacting barchans, using time-resolved cross-plane measurements.

INTRODUCTION

Barchan dunes typically occur in fields with significant heterogeneity in dune size and migration rate (Lancaster, 2009). In this context, the interaction between barchans of different sizes produces complex processes such as collisions, amalgamation and breeding. While the morphology of barchan dunes has been widely studied, the structure of the turbulent flow field associated with barchan dunes, particularly in the wake region, and the role that this modified turbulence plays in barchan interactions remains inadequately understood. In the absence of this understanding, "minimal" models, which lack an adequate simulation of the wake flow structure induced by dunes (e.g. Parteli *et al.*, 2014), remain commonplace, neglecting the role of turbulence and coherent flow structures, and thus struggle to

accurately predict the morphodynamics of barchans when they come in close proximity. This deficiency becomes particularly relevant for dune–dune collisions, when the proximity of an upstream barchan imposes what is essentially a new flow structure over the downstream barchan such that the wake flow needs to be accurately characterized and modelled.

Recent efforts (e.g., Palmer *et al.*, 2012; Wang *et al.*, 2016; Bristow *et al.*, 2018, 2019) have provided important steps forward in this regard. In particular, Bristow *et al.* (2019) suggested the existence of dynamically distinct regions in the barchan wake associated with secondary flows, noting differences in spatial structure downstream of the barchan horns compared with the central region of the wake. This was achieved using analysis of two-point correlations of statistically independent snapshots of the flow the streamwise–spanwise plane.

In the present work, we study the flow field both in the wake of an isolated barchan and in the interdune space of interacting barchans using high frame-rate measurements with three-component stereo PIV in the cross-plane ($y-z$). Such measurements enable analysis of the temporal dynamics by essentially providing a spanwise–wall-normal grid of time-resolved velocity probes through which the spectral content of the flow can be calculated.

EXPERIMENTAL METHODS

Experiments were conducted in the large-scale, refractive-index-matching (LS-RIM) flow facility at the University of Notre Dame. This facility is a scaled-up version of the small-scale refractive-index-matching facility used by Bristow *et al.* (2018), with the LS-RIM cross-section measuring 45 cm×45 cm×2.5 m (i.e., four times larger in both width and height than that of the SS-RIM). The refractive-index-matching (RIM) approach allows full optical access to the entire flow region surrounding three-dimensional models, as they are rendered fully transparent such that the aberrations, reflections, and refraction of light passing through the models are minimized. To achieve RIM, an aqueous solution of Sodium Iodide (NaI) (63% by weight) is used as the working fluid as its refractive index (RI) is very close to that of clear acrylic models. The flow is tripped at the inlet of the test section such that a turbulent boundary layer develops with a thickness of 52.5 mm at the measurement location, resulting in a friction Reynolds number $Re_\tau \approx 1800$.

The barchan models used in the experiments are the same as those used by Bristow *et al.* (2018), which possessed morphologies based on the 3D topography generated by Hersen (2004) and which fit in the range of typical dimensional aspect ratios found in nature. The isolated case utilized this baseline morphology, with which an upstream barchan was then generated having the same shape but half the length, width and height. The first collision stage, hereafter referred to as collision A, featured no deformations to the downstream barchan. In the following two collision stages, hereafter referred to as collisions B and C, the horn of the DBD that is downstream of the upstream barchan was increasingly elongated. All four configurations, including the isolated case and three collision cases, are shown in Figure 1.

Particle-image velocimetry (PIV) was used to measure the flow in the cross-plane ($y-z$) both on the upstream side and in the wake of the large barchan (noted as P1–P4 in Figure 1b) for all four configurations. The flow was seeded with silver-coated solid glass spheres, 2 μm in diameter and $SG = 3.5$, and illuminated with a Northrop Grumman, dual-cavity, Nd:YLF laser. Twelve sets of 2700 image pairs were collected at each measurement location using two 4MP Phantom v641 cameras, fitted with 180 mm Sigma lenses and using Scheimpflug mounts supplied by LaVision. Data was sampled at high frame-rates of 350 Hz in the isolated barchan's wake and 700 Hz in the interdune region (i.e., in the wake of the upstream barchan). The field of view (FOV) covered roughly $4.5H \times 9.5H$ (where H is the height of the large barchan) in the spanwise and wall-normal directions, respectively, while the final PIV interrogation window size of 16×16 pixels^2 and 50% window overlap yielded a grid spacing of approximately 220 μm, or $0.023H$.

RESULTS

As the stereo PIV measurements captured all three velocity components, the full *TKE* spectrum (ϕ_{uu}, ϕ_{vv}, ϕ_{ww}) was calculated (within the limits of the sampling frequency). To that end, the pre-multiplied power spectral density (PSD) at each grid point was computed using fast Fourier transforms (FFT) by the Welch method with 50% overlap, where each time series from a given PIV dataset was divided into shorter segments of 428 time steps. This calculation also involved the use of a cosine-squared "Hanning" tapering window convoluted with each time-series segment to compensate for spectral errors due to side-lobe leakage. The reader is referred to Bendat & Piersol (2011) for further background on these approaches.

The segment length was chosen such that five (5) periods of a time-scale based on a rough estimation of the largest structure of interest within the flow, equal to $10H$ (giving a period length of $10H/U_c$, where U_c is a convection velocity), was sampled within one segment. The convection velocity used in this approximate scaling argument was $0.4U_\infty$ (where U_∞ is the free-stream velocity), which is roughly 90% of the mean streamwise velocity at the larger barchan's height at its centerline. Thus, as there were 11 segments within each time series set of 2700 PIV snapshots, and 12 such sets collected, this yielded 660 samples of a flow structure with a time-scale of $10H/U_c$. Most of the spectral content within the flow field resides at time scales smaller than this, and as such were sampled many more times.

Pre-multiplied power spectral density, $f\phi_{u_iu_j}$, when plotted on a semi-logarithmic scale, allows the identification of the temporal frequencies associated with energetic peaks in the spectral domain. Performing this calculation at every grid point within the FOV allowed for spatial averaging within chosen spanwise domains such that spectrograms could be plotted showing spectral energy as a function of wall-normal position, y, and temporal frequency, f. For the results that follow, the frequency is left unnormalized, since this would typically be done using either a well-defined characteristic time scale or a characteristic convection velocity, U_c, the latter of which can be difficult to determine, particularly for a multi-scale, high *Re* flow such as this. In the previous scaling argument for flow structure sampling, the choice of a convection velocity did not require precision, as it merely set the frequency domain, whereas the use of one throughout the following analysis would introduce significant subjectivity to the results and

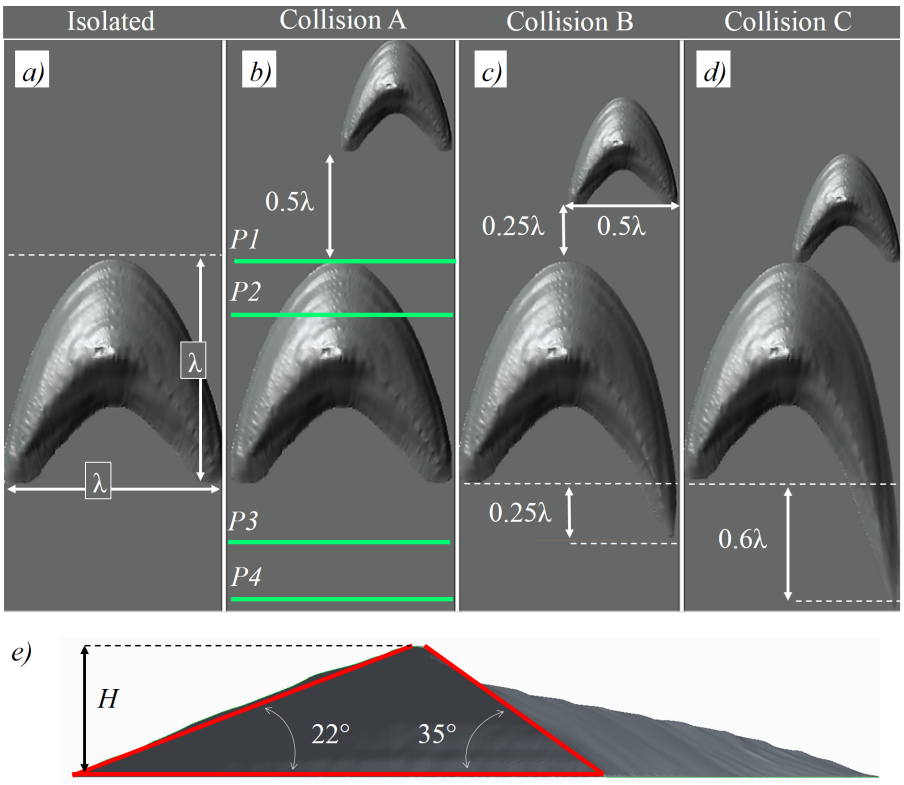

Figure 1. Barchan morphologies and configurations used for the isolated and collision cases. Green lines in (b) and (e) mark the streamwise–wall-normal and streamwise–spanwise measurement plane positions which are the same for all configurations, while in (f) the slopes of the stoss and lee sides are indicated along the dune centerline. Adapted from Bristow *et al.* (2018).

could be misleading.

Isolated barchan wake

Plotting the pre-multiplied *TKE* spectrum, $f\phi_{\mathrm{TKE}} = f(\phi_{\mathrm{uu}}+\phi_{\mathrm{vv}}+\phi_{\mathrm{ww}})$, from streamwise position P3 ($x/H = 5$, at mean reattachment along the centerline) provides a broad overview of the distribution of *TKE* across various frequencies within the wake (Figure 2). The flow field is analyzed in two distinct regions, referred to as Regimes 1 and 2. These refer to spanwise domains for which Regime 1 corresponds to flow downstream of the permanently separated shear layer (i.e., the core of the wake, $|z/H| <= 1.8$) and Regime 2 corresponds to flow downstream of the barchan horns ($1.8 < |z/H| < 3.3$) where the flow is not permanently separated. These two regimes are expected to feature dynamic characteristics unique from one another, based on the results of Bristow *et al.* (2019). In Figure 2, the vertical dashed lines mark a characteristic frequency of flow over the barchan based on its height and the local mean streamwise velocity at its centerline, $\langle U(z/H = 0, y/H = 1)\rangle/H \approx 46$ Hz, as a reference point, while the horizontal dotted lines roughly mark the wall-normal height corresponding to peak pre-multiplied *TKE* spectra.

The most prominent distinctions between Regimes 1 and 2 in the *TKE* spectrum are the concentration of spectral energy near the wall in Regime 2, and the higher magnitude of spectral energy in Regime 1. These characteristics are intuitive, as the topography of the barchan upstream of the measurement position in Regime 1 protrudes much farther into the flow than the topography related to Regime 2. Moreover, since the flow in Regime 1 features a separated shear layer, there is a strong concentration of energy away from the wall. Thus, the spectral content within Regime 2 features more of the near-wall flow structures, and Regime 1 features more energetic vortices shed in the shear layer. Both regimes display a broad *TKE* spectrum at the wall-normal location where their content is highest, but a significant dispersion of spectral energy into the outer flow also exists above their peak frequencies. This demonstrates how unsteady and multi-scale the flow is within each of these regimes, not simply featuring a sharp peak, and a strong influence on the surrounding flow.

The frequencies associated with the peak spectral energy content in Regimes 1 and 2 can be compared by taking a slice of $f\phi_{\mathrm{TKE}}$ at the respective wall-normal height of the broad spectral peak (Figure 3). These individual spectra show more clearly how the most energetic structures in the flow in Regime 2 are skewed towards higher frequencies, while more energy in Regime 1 resides at lower frequencies. Such a result is, in fact, expected from the discussion in Bristow *et al.* (2019), where it was postulated that Regimes 1 and 2 feature different types of flow structures and therefore different associated flow scales. Regime 2, in particular, was argued to have streamwise roller structures that formed due to the morphology of the horns. This notion is expanded upon further by plotting $f\phi_{\mathrm{TKE}}$ from the upstream side of the barchan at P2 (i.e., $x/H = -1$), where, in the same way as for the data from P3, the calculations here are made using data from one side of the centerline, though distinct "regimes" are not defined here. Added to Figure 3a is a profile of $f\phi_{\mathrm{TKE}}$ from a chosen wall-normal height where spectral energy was concentrated (Figure 3c), which shows that the spectral energy peak lies roughly at the same frequency as for Regime 2 at P3. This similarity exists despite the fact that the wall-normal locations where

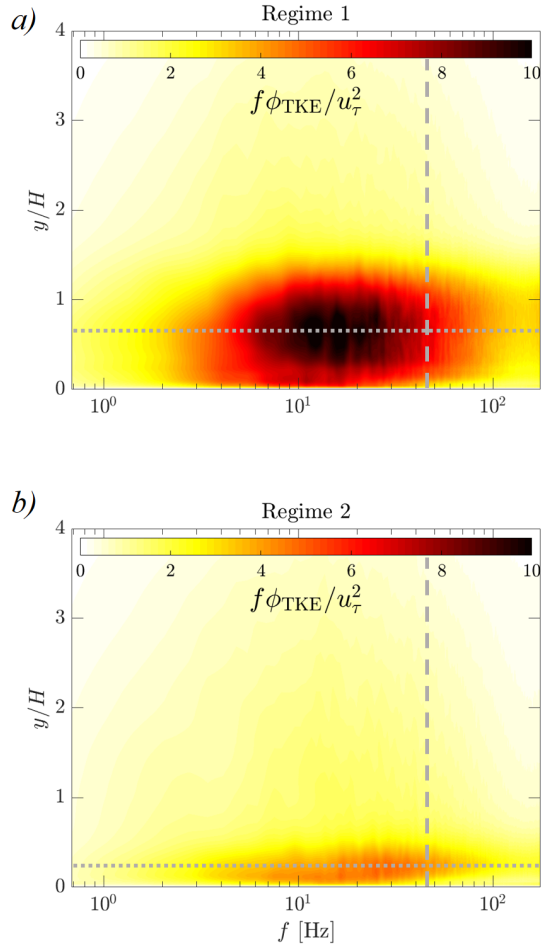

Figure 2. Pre-multiplied *TKE* spectrograms, $f\phi_{\mathrm{TKE}}$, spanwise-averaged in (a) Regime 1, and (b) Regime 2, with data for both from measurement position P3 in the isolated barchan's wake.

the profiles were extracted are at different heights. The inset plot in Figure 3a rescales the y-axis to more clearly delineate the peak from the upstream (P2) data, which can be more difficult to see in the full plot due to its significantly lower maximum value of $f\phi_{\mathrm{TKE}}$ compared to Regimes 1 and 2. From this rescaling, it is apparent that the flow structures measured downstream of the horns in the wake of the barchan are likely formed upstream on its stoss side and persist downstream beyond the horns.

Data from further downstream, in P4 ($x/H = 6.5$), provides additional information about the development of these characteristics of the *TKE* spectra in the wake. Figure 3b presents the data from Regimes 1 and 2 at P3, but now compares with similarly extracted profiles from P4. While the differences between P3 and P4 are not very large, a slight shift in Regime 1 to higher frequencies is noted for P4, while a slight opposite shift in Regime 2 to lower frequencies is noted for P4. This qualitative observation is intuitively consistent with what one might expect further downstream in the wake, where continued mixing and interaction between flow structures renders the characteristic peak frequencies in each regime less distinctly separated. Again, however, it must be noted that these changes are very slight,

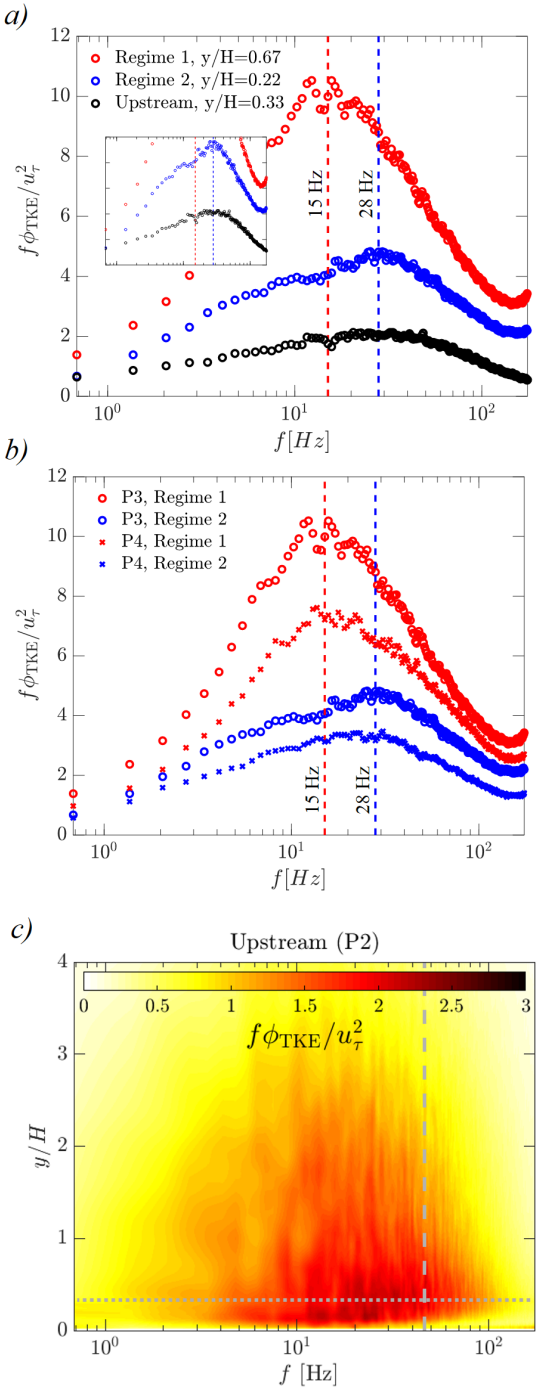

Figure 3. (a–b) Pre-multiplied *TKE* spectra, $f\phi_{\mathrm{TKE}}$, from wall-normal heights corresponding to peak energy content, with (a) comparing Regimes 1 and 2 at P3 in the isolated barchan's wake to data at P2 over the stoss side of the isolated barchan, and (b) comparing Regimes 1 and 2 between positions P3 and P4 in the isolated barchan's wake. (c) Contours of pre-multiplied *TKE* spectra from the stoss side of the isolated barchan, at P2, spanwise-averaged over a region of negative z/H where high levels of $\langle\lambda_{ci}\rangle$ were found.

and for the most part spectra at P4 are very similar to those at P3.

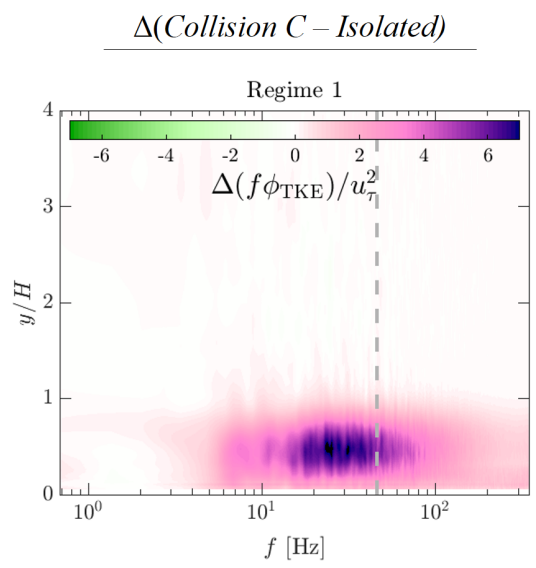

Figure 4. Discrepancy contours of pre-multiplied *TKE* spectra, $\Delta(f\phi_{\mathrm{TKE}})$, comparing data from collision C in Regime 1 at P2 with data from the isolated barchan's stoss side also at P2.

Interdune region

In order to relate these flow structures with sediment transport such that the morphodynamics of the barchan collision process can be better understood, spectral analysis from within the interdune region was utilized. In the context of sediment transport and turbulence, recent work by Diplas *et al.* (2008), Valyrakis *et al.* (2010), and others have demonstrated the importance of the so-called "impulse criterion", which states that two fundamental conditions must be simultaneously met for sediment mobilization to occur. That is, the flow must contain significant energy and this energy must be sustained over a prolonged period. This is precisely what is being described in the spectrograms, plotting pre-multiplied spectral energy ($f\phi$) as a function of a temporal scale (f). Therefore, to assess changes in these terms, discrepancy plots of pre-multiplied *TKE* spectra were computed which compare data from the isolated case to data from collision C (where an upstream barchan is in close proximity), both from P2 (Figure 4). For collision C, only the spectra from Regime 1 of the upstream barchan's wake is used, which is closer to the downstream barchan's surface. The discrepancy between the isolated case and a given collision case is given as

$$\Delta(f\phi) = f\phi|_{col} - f\phi|_{iso}, \tag{1}$$

where "*iso*" and "*col*" refer to data from the isolated and collision cases, respectively, at the same streamwise measurement location. Thus, positive values of $\Delta(f\phi_{\mathrm{TKE}})$ indicate an increase of *TKE* across a range of frequencies due to the presence of the upstream barchan.

Figure 4 illustrates that significant changes in $f\phi_{\mathrm{TKE}}$ occur throughout frequencies spanning roughly a decade in spectral space, between approximately $10-100$ Hz. In this range, $\Delta(f\phi_{\mathrm{TKE}})$ has a maximum magnitude of around 7. For context, the highest magnitude of $f\phi_{\mathrm{TKE}}$ for the isolated case was roughly 2 (Figure 3). The fact that this massive increase in pre-multiplied spectral energy exists down to low frequencies of roughly 10 Hz is noteworthy, as this corresponds to a relatively long time-scale of $\tau_c = 1/f = 0.1$ s. To illustrate this, consider a hypothetical flow structure advecting downstream at a velocity of $0.5U_\infty$. To have a "turnover time" corresponding to $\tau_c = 0.1$ s, the spatial scale associated with this structure would be more than $5H$. In this sense, the flow in the interdune region imposed by the upstream barchan has significant coherence and thus significant sediment mobilization potential due to strong enhancement of *TKE* at frequencies corresponding to long time scales.

CONCLUSIONS

The spectral analysis presented herein has focused on characterizing the differences between flow regimes in the isolated barchan's wake, as well as describing the modified spectral content over the barchan's stoss side due to the presence of an upstream barchan. The results from the isolated barchan showed shifted pre-multiplied spectral peaks depending on the region in the wake being analyzed, suggesting secondary flow structures emanating from the barchan horns which are distinct from the flow in the core of the wake where the flow is permanently separated in the barchan's lee side. Further, these secondary flow structures downstream of the horns appear to be formed on the barchan's stoss side, due to spectral content similarities. These results further support the notions put forward by Bristow *et al.* (2019) suggesting mechanistically distinct flow regimes in the barchan's wake.

In consideration of sediment transport in the interdune region, a comparison between the final collision stage interdune flow and the baseline flow over stoss side of the isolated barchan additionally showed enhancement of *TKE* across a wide frequency band. This was indicated by a large positive *TKE* discrepancy, $\Delta(f\phi_{\mathrm{TKE}})$, with the lower frequency end corresponding to time scales of significant coherence. These results further support the notion of the potential for sediment transport due to the imposition of the upstream barchan's wake, in consideration of an impulse criterion for mobilization.

Further work remains to fully characterize the flow associated with the horns and the separated shear layer of the barchan. Open questions include the instantaneous three-dimensional structure as well as the temporal coherence and persistence of the dominant flow features associated with these regions of the barchan wake.

ACKNOWLEDGEMENTS

This work was supported by the National Science Foundation through collaborative grants CBET-1603211 (Notre Dame) and CBET-1604155 (Illinois).

REFERENCES

Bendat, Julius S & Piersol, Allan G 2011 *Random data: analysis and measurement procedures*, , vol. 729. John Wiley & Sons.

Bristow, N R, Blois, G, Best, J L & Christensen, K T 2018 Turbulent Flow Structure Associated With Collision Between Laterally Offset, Fixed-Bed Barchan Dunes. *Journal of Geophysical Research: Earth Surface* **123** (9), 2157–2188.

Bristow, N. R., Blois, G., Best, J. L. & Christensen, K. T. 2019 Spatial scales of turbulent flow structures associated with interacting barchan dunes. *Journal of Geophysical Research: Earth Surface* p. 10.1029/2018JF004981.

Diplas, Panayiotis, Dancey, Clint L, Celik, Ahmet O, Valyrakis, Manousos, Greer, Krista & Akar, Tanju 2008 The role of impulse on the initiation of particle movement under turbulent flow conditions. *Science* **322** (5902), 717–720.

Hersen, P 2004 On the crescentic shape of barchan dunes. *European Physical Journal B* **37** (4), 507–514.

Lancaster, Nicholas 2009 *Dune Morphology and Dynamics*, pp. 557–595. Dordrecht: Springer Netherlands.

Palmer, Jessica A, Mejia-Alvarez, Ricardo, Best, James L & Christensen, Kenneth T 2012 Particle-image velocimetry measurements of flow over interacting barchan dunes. *Experiments in Fluids* **52** (3), 809–829.

Parteli, E J R, Kroy, K, Tsoar, H, Andrade, J S & Pöschel, T 2014 Morphodynamic modeling of aeolian dunes: Review and future plans. *The European Physical Journal Special Topics* **223** (11), 2269–2283.

Valyrakis, Manousos, Diplas, Panayiotis, Dancey, Clint L, Greer, Krista & Celik, Ahmet O 2010 Role of instantaneous force magnitude and duration on particle entrainment. *Journal of Geophysical Research: Earth Surface* **115** (F2).

Wang, C., Tang, Z., Bristow, N., Blois, G., Christensen, K.T. & Anderson, W. 2016 Numerical and experimental study of flow over stages of an offset merger dune interaction. *Computers & Fluids* **0**, 1–12.